Review article

SeokJae Yoo* and Q-Han Park*

Metamaterials and chiral sensing: a review of fundamentals and applications

https://doi.org/10.1515/nanoph-2018-0167
Received October 3, 2018; revised December 6, 2018; accepted December 11, 2018

Abstract: Chirality, a property of broken mirror symmetry, prevails in nature. Chiral molecules show different biochemical behaviors to their mirror molecules. For left or right circularly polarized lights, the fundamental chiral states of electromagnetic fields interact differently with chiral matter, and this effect has been used as a powerful tool for the detection of chiral molecules. This optical sensing, also termed chiral sensing, is not only easy to implement but also non-invasive to the analytes. However, the measurements made by the optical sensing of chiral molecules are challenging, as chiroptical signals are extremely weak. Recent years have seen active research efforts into metamaterial and plasmonic platforms for manipulating local fields to enhance chiroptical signals. This metamaterial approach offers new possibilities of chiral sensing with high sensitivity. Here, we review the recent advances in chiral sensing using metamaterial and plasmonic platforms. In addition, we explain the underlying principles behind the enhancement of chiroptical signals and highlight practically efficient chiral sensing platforms. We also provide perspectives that shed light on design considerations for chiral sensing metamaterials and discuss the possibility of other types of chiral sensing based on resonant metamaterials.

Keywords: chiral molecules; enantiomers; optical spectroscopy; chiroptical spectroscopy; chiral sensing; plasmonics; metamaterials; circular dichroism (CD); optical rotatory dispersion (ORD).

***Corresponding authors: SeokJae Yoo,** Department of Physics, Korea University, Seoul 02841, Korea; and Department of Physics, University of California, Berkeley, CA 94720, USA, e-mail: seokjaeyoo.nano@gmail.com. https://orcid.org/0000-0002-6438-7123; and **Q-Han Park,** Department of Physics, Korea University, Seoul 02841, Korea, e-mail: qpark@korea.ac.kr

1 Introduction

Metamaterials, artificial materials whose properties cannot be found in natural materials, have been the subject of explosive interest over the past decade because of their ability to manipulate light in both the near- and far-field zones. The most famous example of light manipulation using metamaterials is the negative refraction of light. Metamaterials also allow electromagnetic fields to be strongly confined within a small region, the so-called hot spot, and they are applied to varied fields ranging from molecular sensing [1] to the subwavelength imaging [2]. In addition to the local confinement of light energy, metamaterials are also known to be able to control the phase [3] and spin angular momentum of light [4–6].

Recently, the ability of metamaterials to control light energy and phase has been applied to the chiral sensing of optically active chiral systems. Optical activity is the property of chiral systems of responding to left and right circularly polarized light differently [7]. Optical rotatory dispersion (ORD) and circular dichroism (CD) are typical optical activity phenomena; the former describes the difference in the propagation velocity, and the latter describes the difference in the absorption of two opposite circularly polarized lights. Chiroptical spectroscopy, which measures ORD and CD, has been widely and successfully used in chemistry and biology to obtain important information such as protein secondary structures, electronic transitions of molecules, and conformation of small molecules [7, 8]. Achieving these polarization-dependent chiroptical responses in optically active chiral systems can be aided by the precise local control of light energy and phase allowed by metamaterials. Local phase control is necessary to achieve a circular polarization state at a local region, and the local confinement of light energy should be maximized to enhance the chiroptical signals. In conventional optical spectroscopy, the acquisition of the stereochemical information of chiral systems is hindered by the weakness of chiroptical signals such as ORD and CD. The versatility of metamaterials, including their ability to control local fields, can provide interesting possibilities in the improvement of chiral sensing.

The theoretical [9] and experimental [10] pioneers of chiral sensing demonstrated that the interaction of an optically active system with light can be controlled locally, and this ignited explosive interest in chiral sensing based on metamaterials [11]. Metamaterial researchers have provided metamaterial designs that can enhance chiroptical signals [11–23]. Furthermore, they have also experimentally demonstrated that metamaterials can enhance the chiroptical signals of varied biomolecules whose optically active bands lie in the ultraviolet (UV), visible, and infrared (IR) frequencies [11].

Here, we review the fundamentals and applications of chiral sensing based on metamaterials. In section 2, we briefly explain the basic principles of chiral sensing based on metamaterials. This explanation covers how local fields manipulated by metamaterials can enhance the CD signals of chiral molecules, how chiral molecules and the resonance modes of metamaterials interact with each other, and how chirally fluorescent signals can be modified by optical resonators. In section 3, we introduce the typical chiral sensing metamaterial platforms that have been proposed in recent years. The metamaterial platforms can be categorized into chiral and achiral types according to their structures, and we discuss the advantages and the disadvantages of each platform type. We also introduce non-absorptive methods of chiral sensing using metamaterials, which do not rely on CD measurements. In section 4, we briefly review the experimental demonstrations of various chiral sensing metamaterial platforms. We summarize the correspondence between chiral molecule species and metamaterial platforms for detection. In section 5, we discuss the outlook for chiral sensing platforms and the new possibilities they introduce.

2 Principles of chiral sensing

2.1 Measurement of optical rotational dispersion and CD

CD and ORD measurements are typical optical methods for characterizing chiral molecules. CD is the difference in the absorption of two opposite circularly polarized lights (Figure 1C), while RD is the rotation of the polarization plane of linearly polarized light (Figure 1B). Every polarized plane wave can be decomposed into left and right circularly polarized components $\boldsymbol{E}_{\mathrm{L}}$ and $\boldsymbol{E}_{\mathrm{R}}$. For linearly polarized light, as presented in Figure 1A, the two opposite components have the same magnitudes. When a linearly polarized light beam passes through a chiral sample of finite length, it experiences both ORD and CD. If the chiral sample undergoes ORD without CD, the two components $\boldsymbol{E}_{\mathrm{L}}$ and $\boldsymbol{E}_{\mathrm{R}}$ rotate differently without changing in amplitude, as shown in Figure 1B. On the other hand, the chiral sample with CD preferentially absorbs $\boldsymbol{E}_{\mathrm{L}}$ or $\boldsymbol{E}_{\mathrm{R}}$, and the linearly polarized incident beam becomes an elliptically polarized beam after passing through the sample.

A quantitative understanding of ORD and CD can be made in terms of the polarization-dependent refractive index of the chiral medium. Left (+) and right (–) circularly polarized lights propagating through a medium composed of chiral molecules, i.e. a chiral medium, experience different complex refractive indices $n_{\pm}$. The real and imaginary parts of a refractive index describe the phase evolution and the absorption of the propagating light, respectively. Therefore, CD and ORD for the circular polarized light with the electric field $\mathbf{E}_{0,\pm} = (\hat{\mathbf{x}} \pm i\hat{\mathbf{y}})\exp(in_{\pm}k_0 l)$

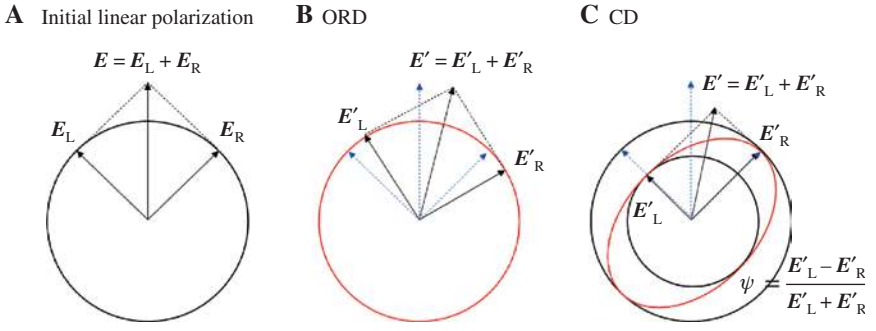

Figure 1: Schematic drawing of ORD and CD.
(A) Initial electric field vector $\boldsymbol{E}$ of the beam before passing through the chiral sample. Final electric field vectors $\boldsymbol{E}'$ of the beams passing through two chiral samples with (B) ORD and (C) CD. Subscripts L and R, respectively, denote the left and right circularly polarized components of the field vector. The initial electric field components are indicated by blue arrows. The polarization ellipses of the final electric fields are depicted by red ellipse. The elliptical polarized beam experienced CD of the sample in Figure 1C can be characterized by the ellipticity $\psi = (\boldsymbol{E}_{\mathrm{L}} - \boldsymbol{E}_{\mathrm{R}})/(\boldsymbol{E}_{\mathrm{L}} + \boldsymbol{E}_{\mathrm{R}})$, where the major and minor axes are given by $\boldsymbol{E}_{\mathrm{L}}$ and $\boldsymbol{E}_{\mathrm{R}}$, respectively.

are, respectively, written in terms of refractive indices as follows [7]:

$$\mathrm{ORD} = \frac{2\pi l}{\lambda}\mathrm{Re}(n_+ - n_-), \tag{1}$$

$$\mathrm{CD} = \frac{2\pi l}{\lambda}\mathrm{Im}(n_+ - n_-), \tag{2}$$

where λ is the wavelength of light and l is the length of the medium. In bulk measurements using a commercial polarimeter, the chiral medium length l corresponds to the length of a cuvette containing the analyte medium.

While the refractive indices for circularly polarized light, $n_\pm$, are macroscopic quantities at the medium level, they have many microscopic origins at the molecular level. For example, natural optical activity is the most fundamental chiroptical property. The molecules have multipole moments including the electric dipole (ED), the electric quadrupole (EQ), and the magnetic dipole (MD). The interference of ED with EQ and MD causes natural optical activity. Note that the interference between EQ and MD is negligible for small chiral molecules because it is a second-order interference in the Rayleigh scattering regime [24]. The ED-EQ interference vanishes for bulk measurements because the rotational averages of molecular orientation cancel the ED contribution in the CD measurement [7, 25], and thus the ED-MD interference plays a pivotal role in the macroscopic chiroptical response of the chiral medium. We can write the ED and MD moments of a chiral molecule induced by the electromagnetic fields in the form $\mathbf{p} = \alpha\mathbf{E} - iG\mathbf{B}$ and $\mathbf{m} = \chi\mathbf{B} + iG\mathbf{E}$ with the electric polarizability α, the magnetic polarizability χ, and the electric-magnetic mixed polarizability G, which is a pseudo-scalar for small chiral molecules. The corresponding macroscopic response of the chiral medium composed of chiral molecules can be described by the following electromagnetic constitutive relations [26]:

$$\mathbf{D} = \varepsilon\mathbf{E} - i\kappa\mathbf{H}, \tag{3}$$

$$\mathbf{B} = \mu\mathbf{H} + i\kappa\mathbf{E}, \tag{4}$$

with the electric field $\mathbf{E}$, and the magnetic field $\mathbf{H}$, the permittivity ε, the permeability μ, and the chirality parameter κ. The relation between the microscopic dipole moments ($\boldsymbol{p}$ and $\boldsymbol{m}$) and the macroscopic constitutive relation ($\boldsymbol{D}$ and $\boldsymbol{B}$) is given by the Clausius-Mossotti relation [26]. Because of the addition of κ-terms in the constitutive relation, two opposite circularly polarized lights become basic propagating waves with the different refractive indices $n_\pm = n \pm \kappa$. Therefore, ORD and CD in molecules with natural optical activity take the following simpler forms:

$$\mathrm{ORD} = \frac{2\pi l}{\lambda}\mathrm{Re}(\kappa), \tag{5}$$

$$\mathrm{CD} = \frac{2\pi l}{\lambda}\mathrm{Im}(\kappa). \tag{6}$$

2.2 Natural optical activity of a small chiral molecule

The optical measurement of molecular chirality is simple and cost-effective, compared to methods featuring atomic resolution, such as STM, HR-TEM, 2D-NRM, and XRD. Therefore, chiroptical spectroscopy is considered the first choice for studying chiral molecular structures. CD and ORD signals are, however, inherently weak in molecules exhibiting natural optical activity. For example, molecular CD signals are 10^{-6} to 10^{-2} of conventional absorption [9, 27]. The extreme weakness of chiroptical signals not only makes it difficult to obtain structural information of high precision but also forces the use of large volumes or high concentration samples for bulk measurement.

To overcome the inherent weakness of chiroptical signals, Tang and Cohen proposed in 2010 that carefully manipulated local electromagnetic fields can enhance the CD signals of a single chiral molecule [9]. They focused on the natural optical activity of a small chiral molecule that only has the ED-MD interference. To calculate the rate of light energy absorption by the molecule at the position $\mathbf{r} = \mathbf{r}_0$, we apply the Poynting's theorem so that [9]

$$A_\pm(\mathbf{r}_0) = \frac{\omega}{2}\{\alpha''|\mathbf{E}(\mathbf{r}_0)|^2 + \chi''|\mathbf{B}(\mathbf{r}_0)|^2\} \pm G''\omega\,\mathrm{Im}\{\mathbf{E}^*(\mathbf{r}_0)\cdot\mathbf{B}(\mathbf{r}_0)\}, \tag{7}$$

for a set of two monochromatic electromagnetic fields under the parity, $\tilde{\mathbf{E}} = \pm\mathbf{E}e^{-i\omega t}$ and $\tilde{\mathbf{B}} = \mathbf{B}e^{-i\omega t}$, whose ellipticities of the polarization states are given by $\pm\psi$, as defined in Figure 1C. The set of two electromagnetic fields introduces the ± sign in Eq. (7). The typical examples of such set of fields are two opposite circularly polarized lights. The subscript ± denotes the parity pair of the fields. The double primes in Eq. (7) indicate the imaginary part. The difference in absorption of the molecule, i.e. CD, is written as follows [9]:

$$\Delta A(\mathbf{r}_0) \equiv A_+(\mathbf{r}_0) - A_-(\mathbf{r}_0) = \frac{4G''}{\varepsilon_0}C(\mathbf{r}_0), \tag{8}$$

where the optical chirality of the field at the position $\mathbf{r} = \mathbf{r}_0$ is defined by $C(\mathbf{r}_0) = -\varepsilon_0\omega\,\mathrm{Im}\{\mathbf{E}^*(\mathbf{r}_0)\cdot\mathbf{B}(\mathbf{r}_0)\}/2$. ε_0 and

ω are the vacuum permittivity and the angular frequency, respectively. In bulk measurements, we measure the ensemble average of Eq. (8). We note that the CD of the single molecule, Eq. (8), can be measured by a single molecule microscopy [28]. In the presence of metamaterial nanostructures, the optical chirality C is often enhanced locally in the vicinity of nanostructures. We will discuss the spatial distribution of C in detail in section 3.

If the chiral molecule is not freely tumbling in the liquid phase or its electric-magnetic mixed polarizability G is no longer pseudo-scalar, the optical chirality defined in Eq. (8) should be modified accordingly. The anisotropy of a molecule can be described by the electric and MD moment along the direction of the unit vectors $\boldsymbol{u}$ and $\boldsymbol{v}$. For the case of anisotropic molecules, $C(\mathbf{r}_0)$ in Eq. (8) is replaced with [15]

$$C(\mathbf{r}_0;\mathbf{u},\mathbf{v}) = -\frac{3\varepsilon_0\omega}{2}\mathrm{Im}[\{\mathbf{u}\cdot\mathbf{E}^*(\mathbf{r}_0)\}\{\mathbf{v}\cdot\mathbf{B}(\mathbf{r}_0)\}]. \tag{9}$$

Metamaterials and plasmonic nanostructures can generate local fields with strong optical chirality, while the optical chirality is fixed to $C_{\mathrm{CPL}} = \pm\varepsilon_0\omega E_0^2/c$ for circularly polarized plane waves with the speed of light in vacuum c. Therefore, the discovery of Eq. (8) has ignited explosive interest in chiral sensing among the metamaterial community [11]. The first experimental demonstration of CD enhancement using metamaterials was a gammadion array proposed by Kadodwala and his coworkers (Figure 1) [10]. On the surface of such gammadion nanostructures, the optical chirality can exceed that of circularly polarized plane waves. They also experimentally demonstrated the CD signals of adsorbed chiral molecules such as α-helical proteins and amino acids. Inspired by this work, many metamaterial designs have been proposed in recent years. We curate and discuss the typical metamaterials in sections 3 and 4.

Let us take a closer look at the mathematical structure of the optical chirality C before concluding this subsection. The optical chirality C is also proportionally related to the optical helicity density h of the monochromatic electromagnetic fields according to the relation $h = C/\omega^2$ [15, 29–31]. The optical helicity density h is more naturally related to other physical quantities, while the optical chirality C is only related to the Lipkin zilch, which is a conserved quantity of electromagnetic fields discovered by Lipkin but has no physical significance [27, 32, 33]. The optical helicity density h of the monochromatic field is defined by

$$h = -\frac{\varepsilon_0\mu_0}{2\omega}\mathrm{Im}(\mathbf{E}^*\cdot\mathbf{H}), \tag{10}$$

The volume integration of the optical helicity density h, i.e. the optical helicity, is a conserved quantity, and the spin angular momentum density $\boldsymbol{s}$ of a light transports the optical helicity density according to the following conservation law:

$$\nabla\cdot\mathbf{s} + \frac{\partial h}{\partial t} = 0, \tag{11}$$

where the spin angular momentum density $\boldsymbol{s}$ of the monochromatic light is defined by

$$\mathbf{s} = \frac{1}{4}\mathrm{Im}(\varepsilon_0\mathbf{E}^*\times\mathbf{E} + \mu_0\mathbf{H}^*\times\mathbf{H}). \tag{12}$$

Each vector component of the spin angular momentum density $\boldsymbol{s}$ also corresponds to the Stokes parameter S_3, which describes the circular polarization state along each direction [29, 34]. For harmonic and monochromatic light, the conservation law, Eq. (11), can be written in the following form [29]:

$$h = \frac{\mathbf{k}\cdot\mathbf{s}}{\omega}, \tag{13}$$

Eq. (13) implies that the optical helicity density h is the projection of the spin angular momentum density $\boldsymbol{s}$ onto the wavevector k. The optical helicity density h can reveal the relation of the molecular CD to the local electromagnetic fields that have the spin angular momentum density $\boldsymbol{s}$ and the Stokes parameter S_3.

2.3 Chiral perturbation of resonance modes

Despite the huge effect of optical chirality on the metamaterial community, it has been reported that experimental results show non-negligible mismatches both between the experiments themselves [10] and with the theoretical predictions based on the local enhancement of the optical chirality [9]. The optical chirality enhancement alone cannot explain the CD enhancement of molecules [11, 13]. When chiral molecules are concentrated in the near-field zone of the resonant metamaterials, they also perturb the resonance modes [11, 13, 35]. As a result of the chiral back action of the molecules on the metamaterials, the electric and magnetic fields in Eq. (7) are no longer the same for two opposite circularly polarized lights, as shown in Figure 2 [13, 35]. Therefore, the absorption rate of a chiral molecule near the resonant structure should be written as follows [13]:

$$A_\pm(\mathbf{r}_0) = \frac{\omega}{2}\{\alpha''|\mathbf{E}_\pm(\mathbf{r}_0)|^2 + \chi''|\mathbf{B}_\pm(\mathbf{r}_0)|^2\} \pm G''\omega\,\mathrm{Im}\{\mathbf{E}_\pm^*(\mathbf{r}_0)\cdot\mathbf{B}_\pm(\mathbf{r}_0)\}. \tag{14}$$

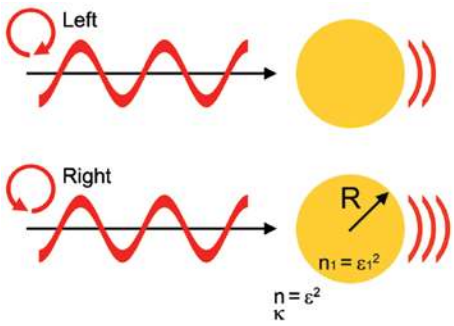

Figure 2: Example of chirally perturbed resonances in nanostructures embedded in the chiral medium. Left and right circularly polarized lights excite the plasmonic nanoparticle differently although the nanoparticle is achiral. Reprinted with permission from Ref. [35], copyright 2015, Nature Publishing Group.

The first two terms in Eq. (14) are not canceled in CD, $\Delta A(\mathbf{r}_0) = A_+(\mathbf{r}_0) - A_-(\mathbf{r}_0)$, resulting in two additional CD components for the chiral molecules coupled to the resonant metamaterials. In addition, the metamaterials also absorb because of lossy elements such as metals. Although the metamaterial structures are not chiral, they chirally absorb the chirally scattered fields caused by nearby chiral molecules. In other words, chirality is transferred to resonant metamaterials from nearby chiral molecules. Therefore, the measured CD signals originate from not only the chiral molecules but also the metamaterials.

We also note that if the chiral effect is included in the numerical algorithm, numerical simulations can predict the total CD signals including chiral back action on resonant metamaterials. Numerical simulations model chiral molecules as a chiral medium whose constitutive relations are given by Eqs. (3) and (4) given the permittivity ε, the permeability μ, and the chirality parameter κ of the medium [13, 36]. The macroscopic constitutive relation of the chiral media can be included into the finite-difference time-domain (FDTD) method [37] and the finite element method (FEM) [36], although numerical stability depends on the method.

2.4 Cavity effect and fluorescence detected circular dichroism (FDCD) and circular luminescence (CL)

Fluorescent chiral molecules exhibit both chiral absorption and chiral emission. When a fluorescent molecule has chiral absorption, i.e. CD, the resulting fluorescent intensity becomes circular dichroic. Measurement of the asymmetric fluorescence intensity is termed FDCD. Both CD and FDCD give the same information about the ground states of chiral molecules [38]. However, the fluorescence of chiral molecules is circularly polarized according to handedness [38–40]. This is called CL, and CL measurements give information about the excited states of the chiral molecules [38].

The modification of emission by optical resonators is a well-known phenomenon, namely, the Purcell effect. In analogy with the Purcell effect, optical resonators have been proven to be able to enhance chiral emissions [15]. The chiral Purcell factor is a measure of the ability of the optical resonator to modify chiral emission and is given by the following [15]:

$$F_C = \frac{1}{4\pi^2}\left(\frac{\lambda_0}{n}\right)^3\left(\frac{Q}{V_C}\right), \tag{15}$$

with the mode wavelength λ_0, the refractive index n, the quality factor of the resonator Q, and the chiral mode volume $V_c = -\omega U/cC_{\max}$. U and $C_{\max}$ are the total energies of the resonator and the maximum optical chirality inside the resonators, respectively. The chiral Purcell factor is exactly the same as the standard Purcell factor, except that the mode volume is replaced by the chiral mode volume. The chiral Purcell factor F_C, Eq. (15), includes the optical chirality term, and thus resonant metamaterials featuring huge C values can enhance the CD, FDCD, and CL of chiral molecules.

3 Metamaterial platforms for chiral sensing

3.1 Chiral metamaterial platforms

The first type of chiral sensing platform is chiral metamaterials. An advantage of using chiral metamaterials is the ease of creating a strong optical chirality C in the vicinity of the chiral metamaterial. As shown in Figure 3, a single sign of the optical chirality C is in spatial excess to the opposite sign on the surfaces of chiral metamaterials.

The gammadion structure in Figure 3A has a strong resonance near the wavelength of 800 nm. At this resonance wavelength, the gammadion structure exhibits CD signals because of its chiral shape. The near-field optical chirality enhancement is also large and uniform, and thus the gammadion structure can strongly couple to chiral molecules. The strong coupling between chiral-shaped gammadions and chiral molecules results

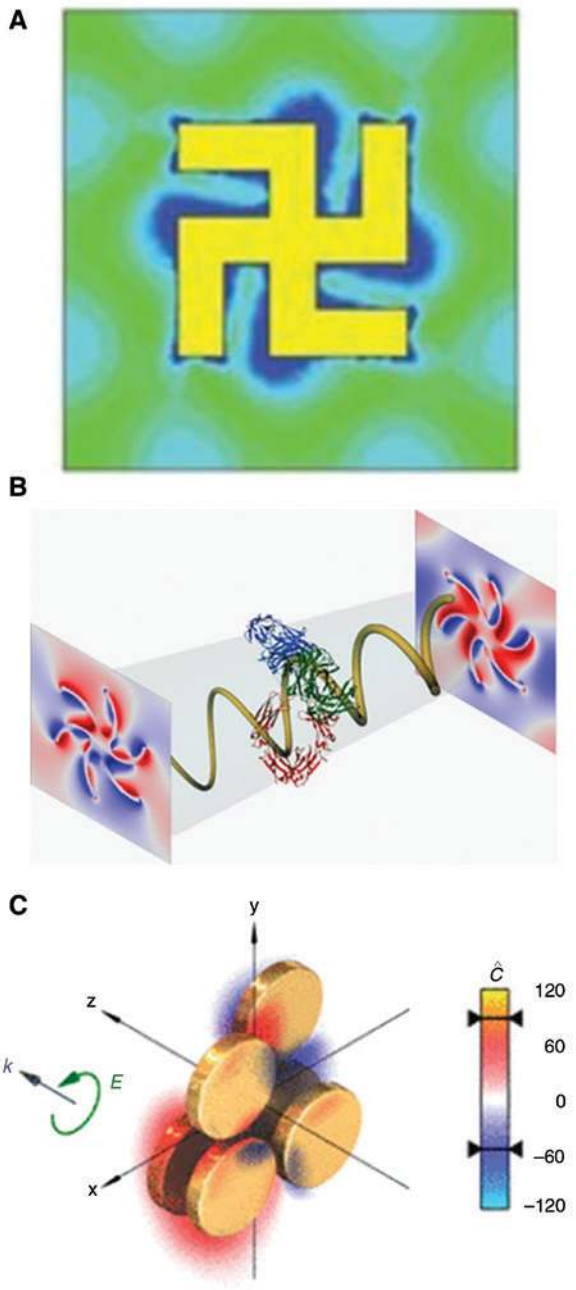

Figure 3: Optical chirality enhancements in the vicinity of various chiral metamaterials and nanostructures: (A) the gammadion structure [10], (B) the shuriken structure [41], and (C) the chiral plasmonic oligomer [17]. Reprinted with permission from Ref. [10], copyright 2010, Nature Publishing Group; Ref. [41], copyright 2018, American Chemical Society; Ref. [17], copyright 2012, American Physical Society.

in different spectral shifts of resonance wavelengths, $\Delta\Delta\lambda \equiv \Delta\Delta\lambda_{RH} - \Delta\Delta\lambda_{LH}$, where $\Delta\lambda_{LH/RH}$ is the wavelength shift of the localized surface plasmon resonance (LSPR) modes according to left-handed (LH) and right-handed (RH) circularly polarized light. For example, β-lactoglobulin coupled gammadions reach up to $\Delta\Delta\lambda = 16$ nm, which is a significantly huge shift.

The Shuriken structure in Figure 3B was applied to characterize a protein interface structure [42] and the structural order of a biointerface [41]. The Shuriken structure has two closely located resonance modes at ~710 nm and ~740 nm. When chiral molecules are ordered on the Shuriken structure surface, the coupling between modes becomes asymmetric. This asymmetric coupling can be used for the chiral sensing for various biomolecules [41, 42].

The plasmonic oligomers in Figure 3C are a plasmonic analog of chiral molecules designed to achieve strong chiroptical response [17]. Simple nanoparticles such as spheres and disks correspond to atoms, and their geometrical arrangements construct plasmonic oligomers. It has been known that plasmonic oligomers can exhibit stronger chiroptical responses than planar nanostructures [17], and they are expected to exhibit strong coupling with chiral molecules. Plasmonic oligomers are also suitable for the fabrication of chiral sensing platforms [43]. It has been shown that twisted nanorods, forming plasmonic oligomers, can enhance the CD signals of 1,2-propanediol [22]. Synthesis of chiral nanoparticles also provides an alternative route to fabricate interesting designs of chiral metamaterial sensing platforms [44], e.g. tetrahedrons with truncations [45], twisted nanorods [44], and nanoparticle helix [43].

Giessen and Schfering also provided some guiding rules for the design of chiral metamaterial platforms [17]. According to their results, a strongly twisted planar structure without sharp corners should be used to obtain a continuous region of enhanced optical chirality. On the other hand, for large differences in optical chirality, a compact three-dimensional chiral structure should be used.

However, chiral metamaterial platforms have limitations because the strong CD signals generated by the platforms themselves can contaminate the relatively weak molecular CD signals [14, 46]. If metamaterial platform structures have chiral geometry, their resonant CD signals are strong even in the absence of chiral molecules. When chiral molecules are loaded to the platform, experimentally measured CD signals have contributions both from molecules and the platform. Therefore, it is hard to distinguish them although chiral metamaterial platform can enhance weak molecular CD. The signs of the molecular CD signals are important because they contain the stereochemical information of the chiral molecules. If we use a chiral metamaterial platform, there is a risk of contaminating the stereochemical information with the strong structural chirality.

3.2 Achiral metamaterial platforms

To overcome the limitations of the chiral metamaterial platform, achiral metamaterials have been suggested as chiral sensing candidates. For single molecule measurements, uniform optical chirality may be unimportant if we can specify the molecular position. For bulk measurement, however, oppositely signed nonuniform optical chirality results in poor CD signals because they can be canceled out by averaging over the whole volume of the metamaterial platform.

An example is the optical chirality enhancements at each corner of the plasmonic nanopatch in Figure 4A [12, 48]. The optical response of many small nanoantennas can be described as a single ED, but the optical chirality distribution of the ED always has opposite signs at the opposite side of the dipole [12]. Nonuniformly signed optical chirality enhancements can also be found in achiral split ring resonators (Figure 4B) [47]. If we want to apply these types of nanostructures to bulk chiroptical measurements, the regions with opposite signs should be blocked by an additional dielectric layer so that only the uncovered regions can host chiral molecules [12]. We also note that optical chirality enhancements of nonuniform sign have been found to preferentially excite the vibrational modes of a right-handed chiral molecule to the extent of its bonds dissociating while leaving a left-handed chiral molecule intact [49].

Figure 4C and D shows metamaterials and nanostructures that can provide a uniform enhancement of optical chirality. The key to achieving optical chirality of uniform sign is the interactions between multiple resonance modes. High-index dielectric nanoparticles (Figure 4C) have multiple resonance modes. If the refractive index of the dielectric nanoparticles is large enough, the well-established hierarchy of the electric and magnetic multipole resonance modes can be found in the visible and IR frequency bands [50]. Interference between multiple modes can provide uniform and same-signed enhancement of optical chirality [46]. The negative refractive index metamaterials presented in Figure 4D also enable uniform optical chirality enhancement [14]. Negative refractive index metamaterials require the simultaneous excitation of electric and magnetic resonances. This characteristic is also a requirement of uniform optical chirality. Recently, an achiral hole-disk coupled array has also been suggested as a chiral sensing platform for enhancing chiroptical signals in the IR regime [51].

Optical chirality enhancement is, however, one of the multiple ways to enhance CD signals using metamaterials.

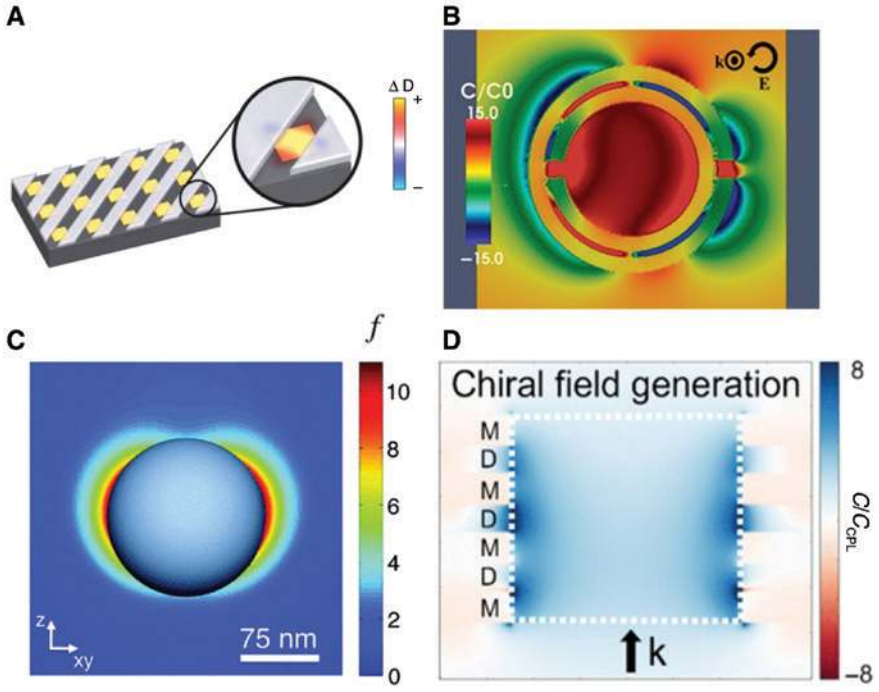

Figure 4: The optical chirality enhancement in the vicinity of various achiral metamaterials and nanostructures: (A) a gold nanopatch array with a cover layer [12], (B) an achiral split ring resonator [47], (C) a silicon nanoparticle [46], and (D) a double fishnet structure [14]. Reprinted with permission from Ref. [12], copyright 2011, Optical Society; Ref. [47], copyright 2015, American Chemical Society; Ref. [46], copyright 2013, American Physical Society; Ref. [14], copyright 2014, American Physical Society.

For example, gold nanospheres [35], nanodisks [13], and half-spheres [19] have nonuniform signs of optical chirality because they only have ED resonances, but they still form enhanced CD signals. In these structures, the resonance modes are perturbed by the adsorbed chiral molecules and become asymmetric under two opposite circular polarized excitations. As presented in Eq. (14) and subsection 2.3, these asymmetrically perturbed resonance modes can give rise to enhanced CD signals. Figure 5 shows the factors contributing to the CD signals of chiral molecules adsorbed only on top of the gold nanodisk array. At the 600-nm wavelength, we find that both CD contributions show clear resonant responses because of the LSPR in gold nanodisks. The CD contribution of gold (red line in Figure 5) is always positive while that of the chiral molecules (green line in Figure 5) changes from negative to positive following the real part of the Lorentzian lineshape. We also point out that the molecular CD contribution is quenched if the chiral molecules are adsorbed across the whole surface of the gold nanodisks due to the non-uniform sign distribution of the optical chirality on the gold nanodisk surface.

3.3 Non-absorptive chiral sensing

3.3.1 Mechanical sorting of chiral molecules

Chiral molecules exhibit not only the chiral absorption of light but also chiral mechanical responses when they are excited by two opposite circularly polarized lights. This allows the sorting of chiral molecules according to their handedness [52–56]. The chiral part of the time-averaged optical force on a chiral molecule whose electric and MD moment are, respectively, described by $\mathbf{d}=\alpha_e\mathbf{E}+i\chi\mathbf{H}$ and $\mathbf{m}=\alpha_m\mathbf{H}-i\chi\mathbf{E}$ is given by the following [52]:

$$\mathbf{F}_c=-\frac{\omega}{g}\mathrm{Re}(\chi)\nabla h-\frac{c}{g}\mathrm{Im}(\chi)(\nabla\times\mathbf{p}-2k^2\mathbf{s})$$
$$-\frac{2\omega}{g}\frac{2k^4}{3n}\{\varepsilon\,\mathrm{Re}(\chi\alpha_m^*)\mathbf{s}_m+\mu\,\mathrm{Re}(\chi\alpha_e^*)\mathbf{s}_e\}, \quad (16)$$

with the prefactor $g=1/4\pi$ in the Gaussian unit system. The formula $h=(g/2\omega)\mathrm{Im}(\mathbf{E}\cdot\mathbf{H}^*)$ is the optical helicity density that is proportional to the optical chirality $C(\mathbf{E},\mathbf{H})$ in the previous section, while $\mathbf{p}=(g/2c)\mathrm{Re}(\mathbf{E}\times\mathbf{H}^*)$ is the momentum density of light and $\mathbf{s}=-(g/4i\omega)\{(\mathbf{E}\times\mathbf{E}^*)/\mu+(\mathbf{H}\times\mathbf{H}^*)/\varepsilon\}$ is the spin angular momentum density of light, which can be decomposed into its electric part $\mathbf{s}_e$ and magnetic part $\mathbf{s}_m$. The terms in Eq. (16) correspond to the chiral parts of the gradient force, the radiation pressure, and the dipole interaction force, respectively [52]. The chiral polarizability χ of the molecule appears in every term in Eq. (16). For a set of two mirror chiral molecule species, their signs of chiral polarizability χ are opposite. Therefore, as shown in Figure 6, the two mirror molecules experience oppositely directed optical forces, and this allows the sorting of chiral molecules according to their handedness.

Although many theoretical suggestions for mechanical sorting of chiral molecules have been made in recent years [52–56], experimental demonstrations are scarce. The first experimental work used spherical droplets of chiral liquid crystal at the micron scale in optofluidic capillary [54]. However, downsizing chiral objects for mechanical chiral sorting requires the beam pitch at wavelength scale with the strong beam intensity. Therefore, the limitation has made the experimental realization of mechanical sorting of nanosize chiral objects impossible so far.

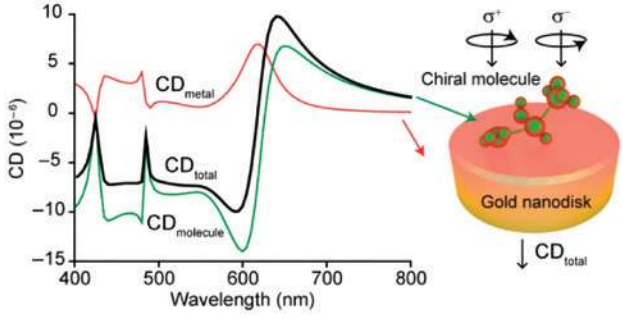

Figure 5: Contributing factors to the CD signals of the gold nanodisk/chiral molecule hybrid system (black line: total CD, red line: CD contribution of the gold nanodisk array, green line: CD contribution of the adsorbed chiral molecules).
Reprinted with permission from Ref. [13], copyright 2018, American Chemical Society.

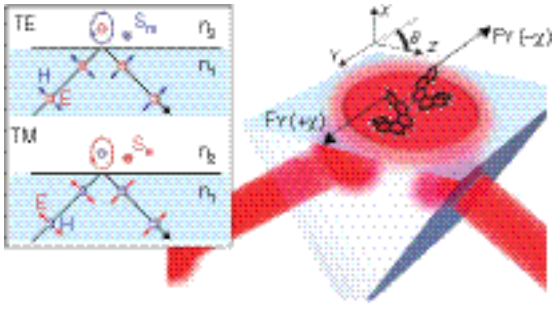

Figure 6: Lateral forces on chiral molecules in an evanescent field.
Reprinted with permission from Ref. [52], copyright 2015, National Academy of Sciences.

3.3.2 Chiral beam splitting

The angle of refraction for a light beam impinging on the chiral medium with refractive indices $n_{\pm}$ is determined by Snell's law as follows [57]:

$$n_0 \sin\theta_0 = n_{\pm} \sin\theta_{\pm}, \tag{17}$$

with the angle of incidence θ_0 and refractive index of the incident medium n_0. Snell's law for the dielectric medium/chiral medium interface implies that the refracted beam is split into two opposite circularly polarized components with different refraction angles $\theta_{\pm}$. The chiral beam splitting based on Eq. (17) is an interfacial effect and does not depend on the length of the sample L, unlike the ORD and CD signals obtained by conventional bulk measurement, which are linearly proportional to L (Eqs. (1) and (2)). This allows the sample volume to be dramatically reduced. For example, a commercial Fresnel lens with micron-scale prism height of 700 μm was used to measure the chiral beam splitting in Figure 7A [57].

Chiral beam splitting-based metamaterial sensing platforms use the photonic spin Hall effect. The photonic spin Hall effect is a photonic analog of the standard spin Hall effect. When a surface has spatial phase gradients, it reflects the incident beam in two opposite directions according to the photonic spin angular momentum of the beam components [5]. On the phase gradient surface, which can enable the photonic spin Hall effect, Snell's law is generalized as follows [4]:

$$n_0 \sin\theta_0 = n_1 \sin\theta_1 - \frac{\lambda}{2\pi}\frac{d\Phi}{dx}, \tag{18}$$

where $d\Phi/dx$ is the phase gradient along the interface and θ_1 is the angle of refraction in the medium whose index is given by n_1. If the periodical phase gradient surface of period P enables the photonic spin Hall effect, the generalized Snell's law, Eq. (18), can be written as [4, 58]

$$\sin\theta_{\pm} = \pm\lambda / P, \tag{19}$$

for the two opposite circularly polarized lights. Shalaev and his coworkers fabricated a 2D array of anisotropic plasmonic nanoantennas to make a surface phase gradient and realize the photonic spin Hall effect shown in Figure 7B [58]. The metasurface presented in Figure 7B has a total thickness of 130 nm because it is only composed of gold nanoantennas on a gold thin film separated by a dielectric spacer. Thus, it strikingly miniaturizes chiral sensing platforms based on beam splitting from the micron-scale to the nano-scale. The angular deviation between the two opposite circularly polarized beams presented in Figure 7C is more pronounced by the new technique using the phase gradient metasurface than the conventional technique presented in Figure 7A.

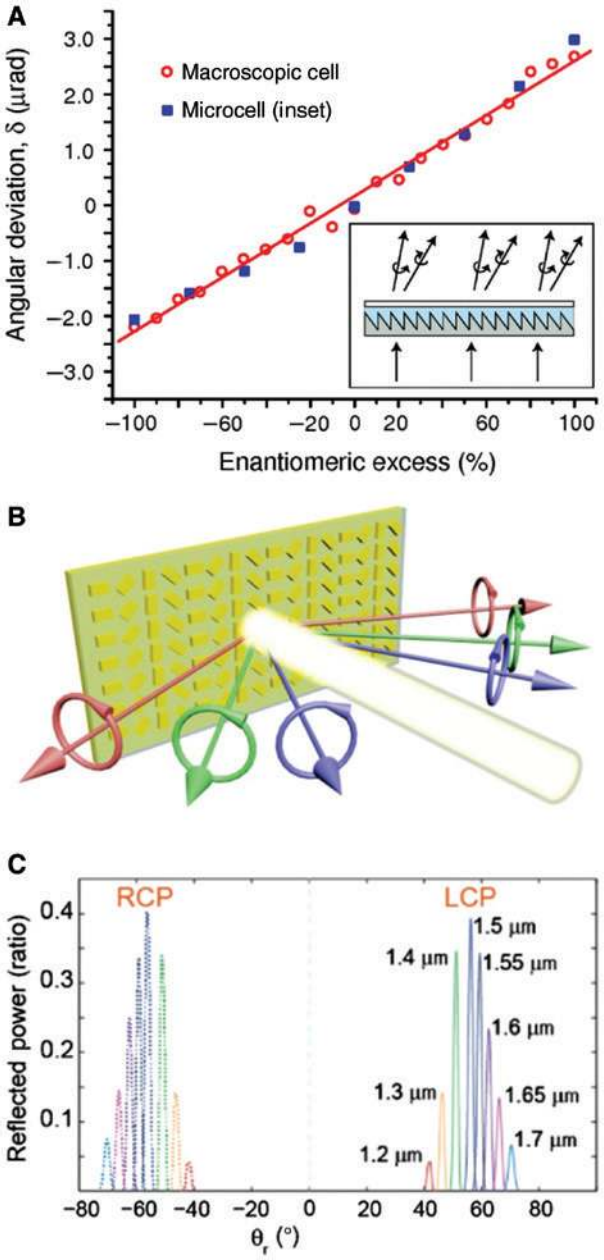

Figure 7: (A) Angular deviation of two refracted beams of opposite helicity in a Fresnel lens filled with limonene at the micron-scale [57]. (B) Schematic of the phase gradient metasurface exhibiting the photonic spin Hall effect [58]. (C) Reflected power of the phase gradient metasurface for two opposite circularly polarized lights. Reprinted with permission from Ref. [57], copyright 2006, American Physical Society; Ref. [58], copyright 2015, Optical Society.

4 Chiral sensing experiments

Researchers have made experimental efforts to detect and characterize chiral molecules using metamaterials and plasmonic structures. In this section, we briefly introduce the molecules that have been successfully detected experimentally using metamaterial chiral sensing platforms. Figure 8 summarizes the molecular chiroptical bands and the metamaterial working bands according to molecular species.

The methods of detecting naturally optically active molecules whose inherent CD signals are in the UV region typically use CD induction in the visible wavelength region by metamaterials and plasmonic structures. In Figure 8, the purple arrows indicate the plasmon-induced CD of chiral molecules whose molecular CD lies in the UV region. For example, the E5 peptide has chiroptical signals at wavelengths near 220 nm, but its mixture with gold nanoparticles (AuNPs) exhibit CD signals at 540 nm, which was the LSPR wavelength of the AuNPs [59]. Similarly, the chiroptical signals of the tobacco mosaic virus at 220 nm [60] and cysteine (Cys) derivatives in the UV bands [61] can induce CD signals in the visible wavelength region when with AuNPs and silver nanoparticles (AgNPs). AuNP clusters feature a large band mismatch between the CD band of Cys and AuNP clusters but exhibit exceptionally huge plasmon-induced CD signals at 800 nm [62]. Cys can form Au-S bonds at the AuNP surface because of its thiol functional group. Once Cys adsorbs on the Au surface, the functionalized AuNPs form clusters due to the Cys-Cys zwitterionic electrostatic interactions between Cys carboxylic and amine groups [62]. In these AuNP clusters, the Cys adsorbed at the gap between two AuNPs can absorb and scatter strong local fields, resulting in the significantly enhanced CD signals at the plasmon resonance wavelengths near 800 nm. Single-stranded (ss) and double-stranded (ds) DNA can be adsorbed on Ag nanocubes, and DNA CD signals in the UV band give birth to plasmon-induced CD signals [63]. In DNA/Ag nanocubes, plasmon-induced CD signals are achieved by strong electric multipole modes rather than an ED mode. If CD signals are induced by higher order plasmon modes, the plasmon-induced CD signals sharpen. Ag nanocubes have also been used to amplify the CD signals of glutathione [64]. We also note that the amino acid and peptide-directed synthesis of chiral plasmonic AuNPs has recently been reported [65]. Chiral organic molecules such as amino acids and peptides adsorbed on the AuNP can introduce enantioselective interactions during AuNP growth and the resulting AuNPs have highly twisted chiral surface structures. The CDs of such chiral AuNPs are extremely strong, and thus the color changes of AuNP colloids with differently polarized light are apparent to the naked eye.

Chiral molecules, which produce chiroptical signals in the visible and near-IR region, can also be enhanced by nanostructures. The CD signals of the riboflavins peak at 360 nm and 450 nm. When riboflavin is coupled to gold nano half dome structures, new CD peaks are induced at the LSPR wavelength (570 nm) and the inherent CD peaks at 360 nm and 450 nm are also enhanced [19]. Another research demonstrated that the metal Shuriken metamaterials resonant at the wavelengths of 693 nm and

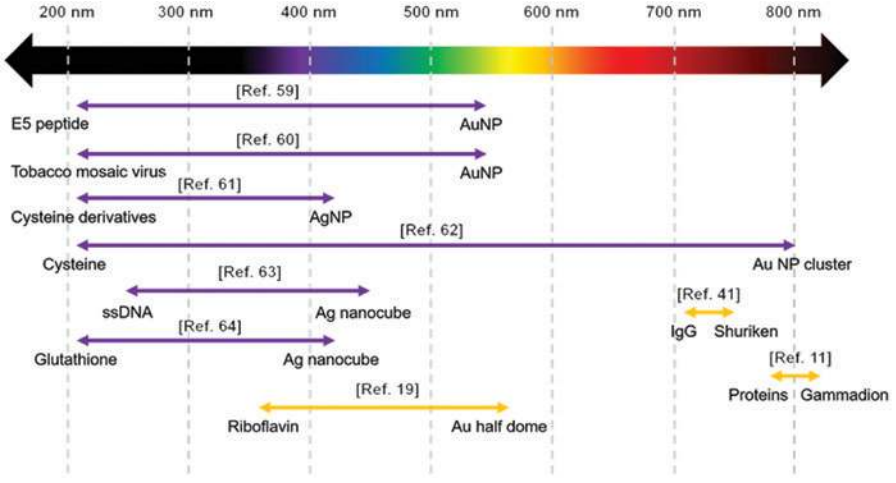

Figure 8: Comparison between molecular chiroptic signal bands and metamaterial working bands from the UV band to the NIR band. Left and right ends of each arrow correspond to the molecular chiroptical and metamaterial working bands, respectively, while the lengths of the arrows indicate the band mismatch between the two bands. Arrow colors indicate molecular chiroptical responses in the UV (purple), visible (orange), and NIR bands (red).

711 nm can detect the ORD signals of immunoglobulin G (IgG) layers at 710 nm and 730 nm [41]. The chiroptical signals of IgG could be used to determine the structural order of IgG on the surface of the metal Shuriken metamaterial. The same research group also showed that the chiroptical signals of α-helical proteins (myoglobin, BSA), β-sheet proteins (OmpA, concanavalin A), and the amino acid tryptophan near at 800 nm can be detected by gammadion metamaterials whose resonances also lie near 800 nm [10]. It also has been shown that twisted metamaterials whose resonance modes are at 500 nm and 1000 nm can detect propanediol and concanavalin A [22]. In the IR region, the vibrational CD of camphor with the wavenumber 3000 cm^{-1} (corresponding to a wavelength of 3.3 μm) could be detected by a gold hole-disk array [51].

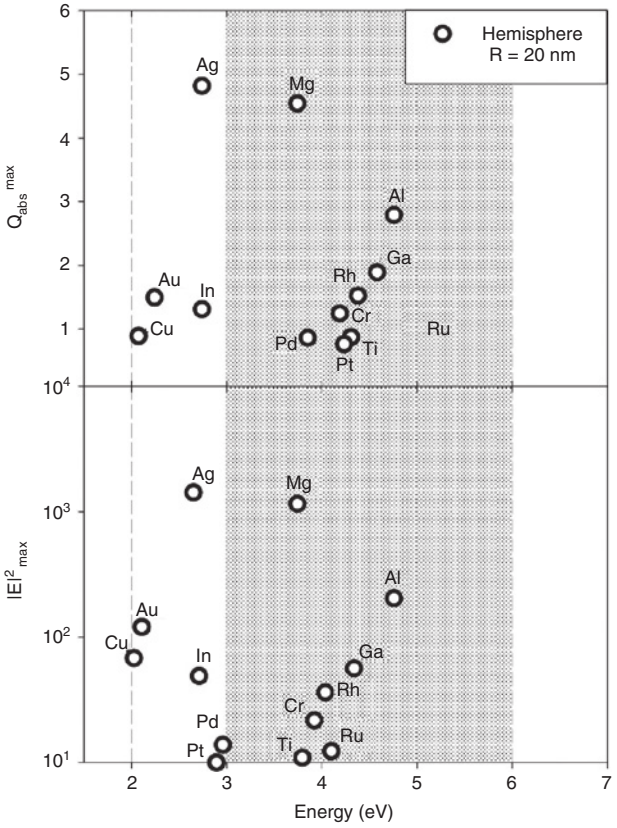

Figure 9: Maximum far-field absorption efficiencies (top) and near-field electric field enhancements caused by the LSPRs in various hemispherical metal nanoparticles of radius R = 20 nm [66]. Reprinted with permission from Ref. [66], copyright 2013, American Chemical Society.

5 Outlook

The most important challenge in chiral sensing based on metamaterials is the band mismatch between the molecular absorption frequencies and metamaterial working frequencies. Chiral molecules with natural optical activity exhibit ORD and CD signals in UV and blue-end visible frequencies, but metamaterials usually work from visible frequencies to IR frequencies. This means that metamaterial chiral sensing platforms have been limited to using the relatively weak ORD and CD signals at non-resonant tails. This band mismatch can restrict the performance of chiral sensing platforms. Limits of the metamaterial working band are caused by two reasons. First, metamaterials are usually composed of plasmonic metal components such as gold and silver. They have interband transitions in the UV region and thus lack UV surface plasmons. However, there are alternative metals that can support UV LSPRs. Figure 9 shows the maximum absorption efficiency and near-field electric field enhancement caused by hemispherical spheres of various metals with a radius of 20 nm [66]. According to Figure 9, aluminum (Al), chromium (Cr), gallium (Ga), indium (In), magnesium (Mg), palladium (Pd), platinum (Pt), rhodium (Rh), ruthenium (Ru), and titanium (Ti) can support strong UV LSPRs and can be used for chiral sensing. For example, it has been demonstrated that Al nanoparticles can enhance molecular CD signals in the UV region [67]. The second reason for limiting the metamaterial working band to the visible frequencies is the difficulty of fabricating subwavelength nanostructures of sizes comparable to UV wavelengths. The top-down lithography technique is also bound by the diffraction limit of light, and thus fabricating nanostructures able to work in the UV region is extremely difficult. On the other hand, recent advances in bottom-up techniques such as DNA origami can achieve nanometer-scale resolution with high precision [68–70] and DNA-aided self-assembly of plasmonic nanoparticles has been demonstrated recently. Such advances have the potential to support chiral sensing in the UV region [70–72].

The previous sections have only focused on the chiroptical interactions between natural optical activity and metamaterials. ORD and CD in small chiral molecules mostly originated from the ED-MD interference. However, in recent years, the metamaterial community has mainly focused on the natural optical activity originating from ED-MD interference. Metamaterials can be applied to various chiral systems with multiple origins. The optical response of physical objects is described by the multipole orders such as the dipole ($n = 1$) and the quadrupole ($n = 2$). The well-established hierarchy of the multipoles helps us to understand the chiroptical responses of objects. The lowest order chiroptical response without external

perturbation includes the ED-MD and ED-EQ interference, and they are known as natural optical activity. In the previous sections, we have only focused on the natural optical activity originating from the ED-MD interference. The ED-EQ interference also contributes to natural optical activity, but it cannot be measured in bulk form because its CD signals vanish due to the rotational averaging of the liquid phase analytes [25]. However, in metamaterial-based chiral sensing, chiral molecules can adsorb on metamaterial surfaces and align in a specific direction. The ED-EQ interference has the same order of magnitude in the multipole hierarchy as the ED-MD interference. Therefore, the light-matter interaction in metamaterials can be studied through the ED-EQ contribution. The time-odd responses of materials are also responsible for the chiroptical signals of materials. Time-odd responses can occur in materials exhibiting properties such as magnetic optical activity, magnetochiral optical activity, and nonreciprocal birefringence [7]. While such effects are small, the ability of metamaterials to manipulate local fields might allow the measurement of chiroptical signals in these types of materials.

Funding: This work was supported by the Samsung Science and Technology Foundation under project no. SSTF- BA1401-05. SeokJae Yoo was supported by the Basic Science Research Program through the National Research Foundation of Korea (NRF) funded by the Ministry of Education (2017R1A6A3A11034238).

References

[1] Brolo AG. Plasmonics for future biosensors. Nat Photonics 2012;6:709–13.
[2] Rogers ETF, Lindberg J, Roy T, et al. A super-oscillatory lens optical microscope for subwavelength imaging. Nat Mater 2012;11:1–4.
[3] Yu YF, Zhu AY, Paniagua-Domínguez R, Fu YH, Luk'yanchuk B, Kuznetsov AI. High-transmission dielectric metasurface with 2π phase control at visible wavelengths. Laser Photonics Rev 2015;9:412–8.
[4] Yu N, Genevet P, Kats MA, et al. Light propagation with phase discontinuities reflection and refraction. Science 2011;334:333–7.
[5] Yin X, Ye Z, Rho J, Wang Y, Zhang X. Photonic spin Hall effect at metasurfaces. Science 2013;339:1405–7.
[6] Shitrit N, Yulevich I, Maguid E, et al. Spin-optical metamaterial route to spin-controlled photonics. Science 2013;340:724–6.
[7] Barron LD. Molecular light scattering and optical activity. Cambridge, England, Cambridge University Press, 2004.
[8] Fasma G. Circular dichroism and the conformational analysis of biomolecules. New York US, Springer, 1996.
[9] Tang Y, Cohen AE. Optical chirality and its interaction with matter. Phys Rev Lett 2010;104:163901.
[10] Hendry E, Carpy T, Johnston J, et al. Ultrasensitive detection and characterization of biomolecules using superchiral fields. Nat Nanotechnol 2010;5:783–7.
[11] Hentschel M, Schäferling M, Duan X, Giessen H, Liu N. Chiral plasmonics. Sci Adv 2017;3:e1602735.
[12] Schäferling M, Yin X, Giessen H. Formation of chiral fields in a symmetric environment. Opt Express 2012;20:26326.
[13] Lee S, Yoo S, Park Q-H. Microscopic origin of surface-enhanced circular dichroism. ACS Photonics 2017;4:2047–52.
[14] Yoo S, Cho M, Park Q-H. Globally enhanced chiral field generation by negative-index metamaterials. Phys Rev B 2014;89:161405(R).
[15] Yoo S, Park Q-H. Chiral light-matter interaction in optical resonators. Phys Rev Lett 2015;114:203003.
[16] Nesterov ML, Yin X, Schäferling M, Giessen H, Weiss T. The Role of plasmon-generated near fields for enhanced circular dichroism spectroscopy. ACS Photonics 2016;3:578–83.
[17] Schäferling M, Dregely D, Hentschel M, Giessen H. Tailoring enhanced optical chirality: design principles for chiral plasmonic nanostructures. Phys Rev X 2012;2:031010.
[18] Yin X, Schäferling M, Metzger B, Giessen H. Interpreting chiral nanophotonic spectra: the plasmonic Born-Kuhn model. Nano Lett 2013;13:6238–43.
[19] Maoz BM, Chaikin Y, Tesler AB, et al. Amplification of chiroptical activity of chiral biomolecules by surface plasmons. Nano Lett 2013;13:1203–9.
[20] Fan Z, Govorov AO. Plasmonic circular dichroism of chiral metal nanoparticle assemblies. Nano Lett 2010;10:2580–7.
[21] Govorov AO, Fan Z, Hernandez P, Slocik JM, Naik RR. Theory of circular dichroism of nanomaterials comprising chiral molecules and nanocrystals: plasmon enhancement, dipole interactions, and dielectric effects. Nano Lett 2010;10:1374–82.
[22] Zhao Y, Askarpour AN, Sun L, Shi J, Li X, Alù A. Chirality detection of enantiomers using twisted optical metamaterials. Nat Commun 2017;8:14180.
[23] Mohammadi E, Tsakmakidis KL, Askarpour AN, Dehkhoda P, Tavakoli A, Altug H. Nanophotonic platforms for enhanced chiral sensing. ACS Photonics 2018;5:2669–75.
[24] Bohren CF, Huffman DR. Absorption and scattering of light by small particles. Weinheim, Germany, Wiley-VCH, 2012.
[25] Tang Y, Cook TA, Cohen AE. Limits on fluorescence detected circular dichroism of single helicene molecules. J Phys Chem A 2009;113:6213–6.
[26] Sihvola AH, Viitanen AJ, Lindell IV, Tretyakov SA. Electromagnetic waves in chiral and bi-isotropic media, US, Artech House, 1994.
[27] Choi JS, Cho M. Limitations of a superchiral field. Phys Rev A 2012;86:063834.
[28] Hassey R, Swain EJ, Hammer NI, Venkataraman D, Barnes MD. Probing the chiroptical response of a single molecule. Science 2006;314:1437–9.
[29] Yoo S. Chiral light-matter interaction in metamaterials. Seoul, Korea, Korea University, 2015.
[30] Bliokh KY, Bekshaev AY, Nori F. Dual electromagnetism: Helicity, spin, momentum and angular momentum. New J. Phys. 2013;15:033026.
[31] Bliokh KY, Bekshaev AY, Nori F. Extraordinary momentum and spin in evanescent waves. Nat Commun 2013;5:14.
[32] Cameron RP, Barnett SM, Yao AM. Optical helicity, optical spin and related quantities in electromagnetic theory. New J Phys 2012;14:053050.

[33] Philbin TG. Lipkin's conservation law, Noether's theorem, and the relation to optical helicity. Phys Rev A 2013;87:1–7.
[34] Setälä T, Shevchenko A, Kaivola M, Friberg AT. Degree of polarization for optical near fields. Phys Rev E 2002;66:1–7.
[35] Yoo S, Park Q-H. Enhancement of chiroptical signals by circular differential mie scattering of nanoparticles. Sci Rep 2015;5:14463.
[36] Lee S, Kang J, Yoo S, Park Q-H. Robust numerical evaluation of circular dichroism from chiral medium/nanostructure coupled systems using the finite-element method. Sci Rep 2018;8:8406.
[37] Akyurtlu A, Werner DH. BI-FDTD: a novel finite-difference time-domain formulation for modeling wave propagation in bi-isotropic media. IEEE Trans Antennas Propag 2004;52:416–25.
[38] Tinoco I, Turner DH. Fluorescence detected circular dichroism. Theory J Am Chem Soc 1976;98:6453–6.
[39] Emeis CA, Oosterhoff LJ. Emission of circularly-polarised radiation by optically-active compounds. Chem Phys Lett 1967;1:129–32.
[40] Schlessinger J, Steinberg IZ, Givol D, Hochman J, Pecht I. Antigen-induced conformational changes in antibodies and their Fab fragments studied by circular polarization of fluorescence. Proc Natl Acad Sci USA 1975;72:2775–9.
[41] Kelly C, Tullius R, Lapthorn AJ, et al. Chiral plasmonic fields probe structural order of biointerfaces. J Am Chem Soc 2018;140:8509–17.
[42] Tullius R, Platt GW, Khosravi KL, et al. Superchiral plasmonic phase sensitivity for fingerprinting of protein interface structure. ACS Nano 2017;11:12049–56.
[43] Kuzyk A, Schreiber R, Fan Z, et al. DNA-based self-assembly of chiral plasmonic nanostructures with tailored optical response. Nature 2012;483:311–4.
[44] Ma W, Xu L, de Moura AF, et al. Chiral inorganic nanostructures. Chem Rev 2017;117:8041–93.
[45] Yeom J, Yeom B, Chan H, et al. Chiral templating of self-assembling nanostructures by circularly polarized light. Nat Mater 2015;14:66–72.
[46] García-Etxarri A, Dionne JA. Surface-enhanced circular dichroism spectroscopy mediated by nonchiral nanoantennas. Phys Rev B 2013;87:235409.
[47] Alizadeh MH, Reinhard BM. Plasmonically enhanced chiral optical fields and forces in achiral split ring resonators. ACS Photonics 2015;2:361–8.
[48] Davis TJ, Hendry E. Superchiral electromagnetic fields created by surface plasmons in nonchiral metallic nanostructures. Phys Rev B 2013;87:085405.
[49] Ho C, Garcia-Etxarri A, Zhao Y, Dionne J. Enhancing enantioselective absorption using dielectric nanospheres. ACS Photonics 2017;4:197–203.
[50] Kuznetsov AI, Miroshnichenko AE, Fu YH, Zhang J, Luk'yanchuk B. Magnetic light. Sci Rep 2012;2:492.
[51] Vázquez-guardado A, Chanda D. Superchiral light generation on degenerate achiral surfaces. Phys Rev Lett 2018;120:137601.
[52] Hayat A, Mueller JPB, Capasso F. Lateral chirality-sorting optical forces. Proc Natl Acad Sci 2015;2015:201516704.
[53] Ding K, Ng J, Zhou L, Chan CT. Realization of optical pulling forces using chirality. Phys Rev A 2014;89:1–7.
[54] Tkachenko G, Brasselet E. Optofluidic sorting of material chirality by chiral light. Nat Commun 2014;5:3577.
[55] Canaguier-Durand A, Hutchison JA, Genet C, Ebbesen TW. Mechanical separation of chiral dipoles by chiral light. New J Phys 2013;15:123037.
[56] Cameron RP, Barnett SM, Yao AM. Discriminatory optical force for chiral molecules. New J Phys 2014;16:013020.
[57] Ghosh A, Fischer P. Chiral molecules split light: reflection and refraction in a chiral liquid. Phys Rev Lett 2006;97:173002.
[58] Shaltout A, Liu J, Kildishev A, Shalaev V. Photonic spin Hall effect in gap-plasmon metasurfaces for on-chip chiroptical spectroscopy. Optica 2015;2:860–3.
[59] Slocik JM, Govorov AO, Naik RR. Plasmonic circular dichroism of peptide-functionalized gold nanoparticles. Nano Lett 2011;11:701–5.
[60] Kobayashi M, Tomita S, Sawada K, et al. Chiral meta-molecules consisting of gold nanoparticles and genetically engineered tobacco mosaic virus. Opt Express 2012;20:24856.
[61] Řezanka P, Záruba K, Král V. Supramolecular chirality of cysteine modified silver nanoparticles. Colloids Surf A Physicochem Eng Asp 2011;374:77–83.
[62] Wang RY, Wang P, Liu Y, et al. Experimental observation of giant chiroptical amplification of small chiral molecules by gold nanosphere clusters. J Phys Chem C 2014;118:9690–5.
[63] Lu F, Tian Y, Liu M, et al. Discrete nanocubes as plasmonic reporters of molecular chirality. Nano Lett 2013;13:3145–51.
[64] Di GMC, Ben MA, Tirosh E, Galantini L, Markovich G. Chiroptical study of plasmon-molecule interaction: the case of interaction of glutathione with silver nanocubes. J Phys Chem C 2015;119:17111–6.
[65] Lee H-E, Ahn H-Y, Mun J, et al. Amino-acid- and peptide-directed synthesis of chiral plasmonic gold nanoparticles. Nature 2018;556:360–5.
[66] Sanz JM, Ortiz D, de la Osa RA, et al. UV plasmonic behavior of various metal nanoparticles in the near-and far-field regimes: geometry and substrate effects. J Phys Chem C 2013;117:19606–15.
[67] McPeak KM, van Engers CD, Bianchi S, et al. Ultraviolet plasmonic chirality from colloidal aluminum nanoparticles exhibiting charge-selective protein detection. Adv Mater 2015;27:6244–50.
[68] Pinheiro AV, Han D, Shih WM, Yan H. Challenges and opportunities for structural DNA nanotechnology. Nat Nanotechnol 2011;6:763–72.
[69] Veneziano R, Ratanalert S, Zhang K, et al. Designer nanoscale DNA assemblies programmed from the top down. Science 2016;352:1534.
[70] Wang P, Gaitanaros S, Lee S, Bathe M, Shih WM, Ke Y. Programming self-assembly of DNA origami honeycomb two-dimensional lattices and plasmonic metamaterials. J Am Chem Soc 2016;138:7733–40.
[71] Urban MJ, Dutta PK, Wang P, et al. Plasmonic toroidal metamolecules assembled by DNA origami. J Am Chem Soc 2016;138:5495–8.
[72] Liu W, Halverson J, Tian Y, Tkachenko AV, Gang O. Self-organized architectures from assorted DNA-framed nanoparticles. Nat Chem 2016;8:867–73.